HHS Public Access

Author manuscript

Biochemistry. Author manuscript; available in PMC 2021 June 10.

Published in final edited form as:

Biochemistry. 2020 November 24; 59(46): 4470–4480. doi:10.1021/acs.biochem.0c00755.

Enterococcus NlpC/p60 peptidoglycan hydrolase SagA localizes to sites of cell division and only requires catalytic dyad for protease activity

Juliel Espinosa[1], **Ti-Yu Lin**[1], **Yadyvic Estrella**[1], **Byungchul Kim**[1], **Henrik Molina**[2], **Howard C. Hang**[1,3,*]

[1]Laboratory of Chemical Biology and Microbial Pathogenesis, The Rockefeller University, New York, New York 10065, United States.

[2]Proteomics Resource Center, The Rockefeller University, New York, New York 10065, United States.

[3]Departments of Immunology & Microbiology and Chemistry, Scripps Research, La Jolla, California 92037, United States.

Abstract

Peptidoglycan is a vital component of the bacterial cell wall, and its dynamic remodeling by NlpC/p60 hydrolases is crucial for proper cell division and survival. Beyond these essential functions, we previously discovered that *Enterococcus* species express and secrete the NlpC/p60 hydrolase secreted antigen A (SagA), whose catalytic activity can modulate host immune responses in animal models. However, the localization and peptidoglycan hydrolase activity of SagA in *Enterococcus* was still unclear. In this study, we show that SagA contributes to a tri-septal

[*]**Corresponding Author:** hhang@scripps.edu.

Howard C. Hang − Laboratory of Chemical Biology and Microbial Pathogenesis, The Rockefeller University, New York, New York 10065, United States; Departments of Immunology and Microbiology and Chemistry, Scripps Research, La Jolla, California 92037, United States

Juliel Espinosa − Laboratory of Chemical Biology and Microbial Pathogenesis, The Rockefeller University, New York, New York 10065, United States

Ti-Yu Lin − Laboratory of Chemical Biology and Microbial Pathogenesis, The Rockefeller University, New York, New York 10065, United States

Yadyvic Estrella − Laboratory of Chemical Biology and Microbial Pathogenesis, The Rockefeller University, New York, New York 10065, United States

Byungchul Kim − Laboratory of Chemical Biology and Microbial Pathogenesis, The Rockefeller University, New York, New York 10065, United States

Henrik Molina – Proteomics Resource Center, The Rockefeller University, New York, New York 10065, United States

The authors declare no competing financial interest.

Accession Codes

E. faecium Com15 *sagA* (NCBI, WP_127808574.1); *E. durans* 23C2 *sagA* (NCBI, WP_016177750.1); *E. mundtii* NCDO 2375 *sagA* (NCBI, WP_023520500.1).

ASSOCIATED CONTENT

Supporting information

The Supporting Information is available free of charge via the internet

Fluorescence microscopy, transmission electron microscopy, intact protein MALDI-TOF MS analysis, total ion chromatograms of data shown in Figure 3C and further quantification of *in vitro* SagA D,L-endopeptidase activity, 2D ligand interaction diagram, *in silico* alanine scanning, total ion chromatograms of data shown in Figure 5C, multiple sequence alignment and structural alignment of SagA-NlpC/p60 with the NlpC/p60 domains of biochemically and structurally characterized NlpC/p60 proteins, bacterial strains and plasmids used in this study, predicted binding free energies of highest-scoring poses from docking study, molecular mass and composition of soluble *E. faecalis* OG1RF PG and enzymatic products from incubation with purified SagA constructs. (PDF)

structure in dividing enterococci cells and localizes to sites of cell division through its N-terminal coiled-coil domain. Using molecular modeling and site-directed mutagenesis, we identify amino acid residues within the SagA-NlpC/p60 domain that are crucial for catalytic activity and potential substrate binding. Notably, these studies revealed that SagA may function via a catalytic Cys-His dyad instead of the predicted Cys-His-His triad, which is conserved in SagA orthologs from other *Enterococcus* species. Our results provide key additional insight into peptidoglycan remodeling in *Enterococcus* by SagA NlpC/p60 hydrolases.

Graphical Abstract

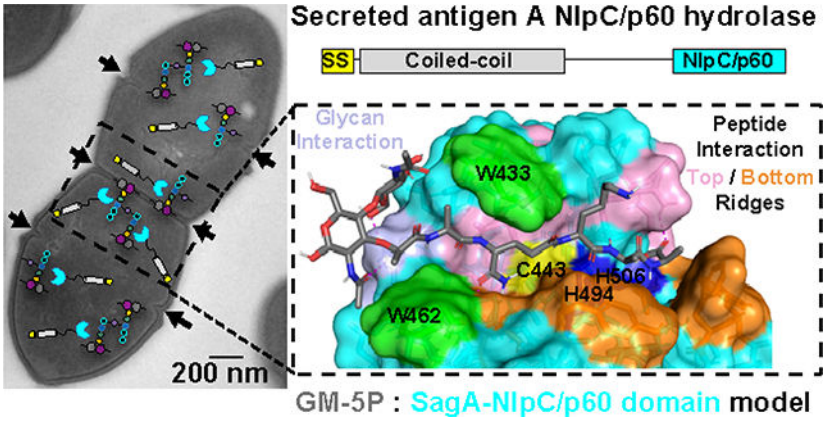

INTRODUCTION

Peptidoglycan (PG) is a vital component of the bacterial cell wall, and its dynamic remodeling is crucial for proper cell growth, division, and survival.[1] Moreover, these cell wall fragments from commensal and pathogenic bacteria can activate host immune signaling pathways.[2–6] However, the mechanism(s) by which immunologically active peptidoglycan fragments are generated are not well-understood.[6] In this regard, PG hydrolases are ubiquitous in bacteria and possess diverse activities to cleavage of internal peptide stem linkages for peptidoglycan remodeling during cell growth and division.[7,8] In the process of remodeling the cell wall, these PG hydrolases can also generate non-crosslinked muropeptides that are shed or recycled and available for triggering host immune responses through pattern recognition receptors such as nucleotide-binding oligomerization domain containing (NOD) 1 and 2 proteins or inflammasomes.[4–6] Indeed, our laboratory has shown that a NlpC/p60-type PG hydrolase also termed secreted antigen A (SagA) from *Enterococcus faecium* (*Efm*), confers pathogen tolerance to *Caenorhabditis elegans* as well as protects mice against enteric pathogens such as *Salmonella* Typhimurium and *Clostridium difficile*.[9,10]

SagA is a ~55 kDa protein comprised of a secretion-signal peptide and three domains: a coiled-coil N-terminus, serine/threonine-rich linker, and NlpC/p60[11] C-terminus with a conserved putative catalytic triad (Cys443, His494 and His506).[9] To characterize the key amino acid residues necessary for PG hydrolytic activity, our laboratory embarked on structural and biochemical studies of recombinant SagA C-terminal domain (i.e. SagA-

NlpC/p60).[12] The structure of the SagA-NlpC/p60 domain (PDB 6B8C) was solved to 2.4 Å resolution by X-ray crystallography. LC-MS/MS analysis of PG extracts and isolated muropeptides incubated with SagA-NlpC/p60 demonstrated that it specifically cleaves muramidase-predigested but not intact L-Lys type PG. SagA-NlpC/p60 preferentially cleaves cross-linked PG fragments with penta- and tetrapeptide stems found in nascent PG chains.[12] We observed that Trp433 and Trp462 protrude prominently from the SagA-NlpC/p60 structure and may serve as clamps for binding potential peptidoglycan substrates. Alanine mutants of Cys443, Trp433, and Trp462 abolished the D,L-endopeptidase activity of SagA-NlpC/p60.[12] Moreover, the isolated disaccharide-dipeptide cleavage product, GlcNAc-MurNAc-L-Ala-D-isoGln (GlcNAc-MDP), was shown to activate NOD2 in mammalian cells in a dose-dependent manner.[12] Remarkably, heterologous expression and secretion of SagA in the probiotic bacterium, *Lactobacillus plantarum*, was sufficient to confer protective activity *in vivo*, highlighting the therapeutic potential of SagA.[9,10,12]

These findings have improved our understanding of the mechanisms that govern SagA-mediated protection, yet the localization of SagA in *Efm* and its ligand-protein interactions remain elusive. A major constraint toward elucidating the precise function of SagA is its essential role in *Efm* division and growth, as complementation of *sagA* was required for disruption of the chromosomal gene.[13] Also, the structural basis of the direct contacts between PG substrates and SagA is key to understanding how the D,L-endopeptidase activity of *Efm* SagA functions *in vivo*, possibly on other bacteria or dietary PG fragments. Obtaining a muropeptide-bound structure of SagA to reveal these significant contacts, however, has proven challenging; the preferred muropeptide substrates of SagA are large and cross-linked, and purification of these fragments for crystallization trials is limiting.

To address these outstanding questions, we embarked on imaging studies of enterococci and SagA as well as additional structure activity studies. Using a fluorescent analog of D-alanine to probe for actively growing cells as well as transmission electron microscopy (TEM), we showed that SagA contributes to a tri-septal structure in dividing SagA+ enterococci cells. Fluorescence microscopy of tetracysteine (Cys4)-tagged SagA and its truncation constructs overexpressed in *Efm* Com15 revealed that SagA is localized at the cell division site via its coiled-coil N-terminus, which suggests that SagA is involved in PG remodeling during cell division. Moreover, comparison of the biochemical activity of recombinant full-length SagA and the SagA-NlpC/p60 showed that the N-terminus does not appear to have an auto-inhibitory function. Molecular docking studies of the SagA-NlpC/p60 structure with a representative monomeric pentapeptide PG fragment revealed key features of the putative SagA-NlpC/p60 substrate binding groove. Subsequent alanine-scanning mutagenesis of potential key residues of SagA-NlpC/p60 *in vitro* afforded additional insight to SagA D,L-endopeptidase activity in enterococci during cell division. In addition, we discovered that full-length SagA orthologs from several other *Enterococcus* species exhibit D,L-endopeptidase activity *in vitro* via a Cys-His catalytic dyad. Our investigation of SagA localization and biochemical activity highlights how SagA is involved in remodeling the cell wall in *Enterococcus*, which is important for understanding its roles in bacterial cell division and modulation of host immune responses.

MATERIALS AND METHODS

Plasmid constructions.

Cloning and transformations.—All cloning was done in chemically competent *E. coli* Dh5α (New England Biolabs, NEB) according to the manufacturer's protocol (pAM401 plasmids = 25 μg mL^{-1} chloramphenicol; pET-21a(+) plasmids = 100 μg mL^{-1} ampicillin). Colonies were picked and verified by Sanger sequencing (Genewiz). Confirmed pAM401 plasmids were transformed into electrocompetent *Efm* Com15 (Table S1) according to a Palmer laboratory *Enterococci* transformation protocol[14] for constitutive expression (10 μg mL^{-1} chloramphenicol). Confirmed pET-21a(+) plasmids were transformed into competent *E. coli* BL21-CodonPlus (DE3)-RIL (Agilent) according to the manufacturer's protocol for IPTG inducible expression (100 μg mL^{-1} ampicillin *and* 25 μg mL^{-1} chloramphenicol; see note in Table S1).

Plasmid constructions for fluorescent microscopy.—The Tetracysteine (Cys_4) Tag[15,16] was inserted into pAM401 plasmids containing *Efm* Com15 *sagA* (NCBI, WP_127808574.1) and its variants[9] by using the QuikChange XL site-directed mutagenesis kit (Stratagene) according to the manufacturer's protocol. To create *SagA-Cys$_4$-His$_6$*-pAM401, *SagA-His$_6$*-pAM401 was used as the template (**Table 1**) along with primers 1 and 2 (Table S2). To create $SagA^{\Delta C}$-*Cys$_4$-His$_6$*-pAM401, $SagA^{\Delta C}$-*His$_6$*-pAM401 was used as the template along with primers 3 and 4. To create $SagA^{Nter}$-*Cys$_4$-His$_6$*-pAM401, $SagA^{Nter}$-*His$_6$*-pAM401 was used as the template along with primers 5 and 6. Transformation into *E. coli* Dh5α and subsequent transformation into *Efm* Com15 performed as described above.

Plasmid constructions for protein expression.—Site-directed mutagenesis of *Efm* Com15 SagA constructs in the pET-21a(+) vector backbone (Millipore Sigma) was performed using Q5 Hot-Start High-Fidelity 2x master mix (NEB) according to the manufacturer's protocol. To generate individual alanine mutants of *Efm* Com15 SagA-NlpC/p60, *Efm*_Com15_SagA-NlpC/p60_ΔSS-His_6-pET-21a(+)[12] was used as a template (Table S1) along with the appropriate primer pairs from primers 7–36 (Table S2). To generate signal sequence deletion mutants of full-length *Efm* Com15 SagA WT and C443A, *Efm*_Com15_SagA-His_6-pET-21a(+)[9] and *Efm*_Com15_SagA_C443A-His_6-pET-21a(+)[12] were used as templates, respectively, along with primers 37 and 38. To generate the full-length *Efm* Com15 SagA ΔSS H506A mutant, *Efm*_Com15_SagA_ΔSS-His_6-pET-21a(+) was used as a template along with primers 35 and 36. Transformation into *E. coli* Dh5α and subsequent transformation into *E. coli* BL21-CodonPlus (DE3)-RIL performed as described above.

To clone signal sequence deletion mutants of full-length SagA orthologs, genomic DNA from *E. durans* 23C2 and *E. mundtii* NCDO 2375 was purified from 5 mL overnight cultures using the E.Z.N.A. Bacterial DNA Kit (Omega Bio-Tek) according to the manufacturer's protocol. *E. durans* 23C2 *sagA* (NCBI, WP_016177750.1; primers 39 and 40) and *E. mundtii* NCDO 2375 *sagA* (NCBI, WP_023520500.1; 41 and 42) were amplified as signal sequence deletion mutants from the respective genomic DNA samples using Q5 Hot-Start High-Fidelity 2x master mix according to the manufacturer's protocol. Sequences were

inserted into the pET-21a(+) plasmid that was double digested with NdeI (NEB) and XhoI (NEB) using the NEBuilder HiFi DNA Assembly Cloning Kit (NEB). Transformation into *E. coli* Dh5α and subsequent transformation into *E. coli* BL21-CodonPlus (DE3)-RIL performed as described above.

Western blot analysis of bacterial supernatants and pellets, and purified proteins.

Western blot analysis of bacterial supernatants and pellets, and purified proteins performed as described previously.[12,17]

Fluorescence microscopy.

Cells were grown to log phase (OD_{600}~0.6) and labeled with 5 mM HADA (TOCRIS) and 10 μM ReAsH (Invitrogen) in BHI for 30 mins, followed by two washes with PBS to remove excess dye. We fixed the cells with 1% formaldehyde for 10 mins and washed and resuspended the cells with PBS. All the procedures were performed at room temperature.

To image cells, an aliquot of cell suspensions was transferred to the surface of a 2% (wt/vol) agarose pad prepared in PBS, covered with a glass coverslip, and imaged with a DeltaVision Image Restoration Microscope (Applied Precision) using DAPI (4',6-diamidino-2-phenylindole) and AlexaFluor 594 filters. Cells for TEM were prepared as described previously.[12]

Protein expression and purification, and *in vitro* activity assays.

Recombinant SagA-NlpC/p60 mutants and full-length SagA orthologs were expressed and purified as described previously.[17] *In vitro* activity assays were performed as described previously,[17] with modifications included below.

Liquid chromatography.—For each sample, 10 μL was injected onto a C18 reversed phase column [Acclaim 120 C18 3um 2.1 × 150mm (DX059130)] at 176 μL/min and kept at 52°C using an isocratic gradient. The molecules were eluted using a gradient increasing from 0% B / 100% A to 100% B / 0% A in 59 minutes (Buffer A: 0.1% TFA, Buffer B: 30% Methanol/0.1% TFA). Solvent composition was held at 100% B / 0% A for 5 minutes where after the column was conditioned for 5 minutes at 0% B / 100% A. All solvents were LCMS grade.

Mass spectrometry.—Reversed phase separated molecules were measured in MS mode using an Orbitrap XL operated at 60,000 resolution (Auto Gain Control of 1–2e5 and maximum injection time of 500 ms). Collision Induced Dissociation MS/MS spectra were acquired in ion trap mode (AGC of 1e4 and maximum injection time of 25 ms) fragmenting 1 or 2 of the most abundant ions per cycle.

Intact protein analysis by Matrix-assisted Laser Desorption Time-of-Flight Mass Spectrometry.

1 μL of the sample was mixed with 9 μL of matrix consisting of a saturated solution of α-cyano-4-hydroxycinnamic acid (4-HCCA) in a 1:3:2 (v/v/v) mixture of formic acid/water/isopropanol (FWI). An aliquot of 0.5 – 1 μL of this protein-matrix solution was spotted onto

a MALDI plate precoated with an ultrathin layer of 4-HCCA matrix.[18,19] The sample spots were then briefly washed for a few seconds with 2 μL of cold 0.1% aqueous trifluoroacetic acid (TFA) solution and vacuum suction. MALDI spectra were acquired in linear, delayed extraction mode using a Spiral TOF JMS-S3000 (JEOL, Tokyo, Japan). The instrument is equipped with a Nd:YLF laser, delivering 10-Hz pulses at 349 nm. Delayed extraction time was set at 0.75 – 1 μs and acquisition was performed with a sampling rate of 2 ns. The MALDI spectrum consists of an average of 500 scans. Horse myoglobin was used as a mass calibrant with a technique of pseudo-internal calibration wherein a few laser shots on a calibrant spot near a sample spot were collected and averaged with the sample shots into a single spectrum. The spectra were processed and analyzed using MoverZ (Proteometrics, LLC).

Secondary structure homology modeling.

The secondary structure homology of the *Efm* Com15 SagA N-terminus (residues 27–268) was evaluated by submitting the sequence to Phyre2.[20] The confidence is reported, or the probability that the match between the *Efm* Com15 SagA N-terminus sequence and the top hit, *Streptococcus pneumoniae* PcsB,[21] is based on predicted secondary structure and sequence identity.

Molecular docking.

The Grid-based Ligand Docking with Energetics (GLIDE) module of the Schrödinger suite was used to generate a list of poses with highest scores[22,23] similar to our previously described docking studies.[12] The raw SagA-NlpC/p60 structure was first prepared for the docking study using the Schrödinger Preparation Wizard and then aligned to the NlpC/p60 domain of the *Bacillus cereus* YkfC structure (PDB: 3H41). The ligand recognition site in SagA-NlpC/p60 was centered on the L-Ala-γ-D-isoGlu dipeptide bound to BcYkfC-NlpC/p60. The docking search space was specified by setting the ligand diameter midpoint cubic box to 10 × 10 × 15 $Å^3$, which broadly covers the solvent exposed groove of SagA-NlpC/p60. Standard parameters were applied including van der Waals (vdW) scaling of nonpolar atoms (by 0.7) to include modest ‘induced fit’ effect of ligand. The molecular docking of SagA-NlpC/p60 with the GlcNAc-MurNAc-L-Ala-D-isoGln-L-Lys-D-Ala-D-Ala ligand was done in a flexible, non-constrained manner and restricted to the reference position of the L-Ala-γ-D-isoGlu dipeptide bound to BcYkfC-NlpC/p60; the inclusion of this restriction allowed the GlcNAc-MurNAc and D-Ala-D-Ala groups to rotate freely within the volume of the grid box. All other settings were kept as default. Docking simulations were performed in two steps, which included initial validation of the standard precision (SP) docking algorithms to predict the most accurate binding of ligand with apo SagA-NlpC/p60 structure, and then molecular mechanics generalized born surface area (MM-GBSA) calculations of binding free energies of top-ranked ligand poses (Table S3).[24]

Residue scanning.

The residue scanning panel was used in Schrödinger to produce the following mutated structures: SagA-NlpC/p60 Y493A, SagA-NlpC/p60 H506A, and SagA-NlpC/p60 E512A. A Prime side-chain prediction with backbone sampling was performed to refine the mutated residue and nearby residues in each mutant structure.

Structure alignment.

The *align* function was used in PyMOL v2.3.5 (Schrödinger) to perform a sequence alignment followed by structural superposition of NlpC/p60 orthologs.

RESULTS & DISCUSSION

According to the template model of PG assembly in enterococci, actively dividing cells generate nascent PG chains at the septum with non-crosslinked pentapeptide stems, which are trimmed in mature PG by an L,D-carboxypeptidase.[25–27] To determine if SagA plays a role in PG remodeling, we stained *Efm* cells with HADA,[28] a D-alanine analog containing a fluorescent coumarin moiety that has been used to probe newly synthesized PG in many bacterial species (Figure 1A). We found that dividing *Efm* cells show a tri-septal HADA staining pattern labeling the septa and equators (Figure 1B–D). In contrast, *Enterococcus faecalis* (*Efs*), which does not have a *sagA* gene, only exhibited HADA staining at the division septa. However, an *Efs* OG1RF strain expressing SagA (*Efs-sagA*[9]) revealed HADA staining at both septa and equators, suggesting a role of SagA in PG remodeling during cell division. The tri-septal structure was also confirmed by transmission electron microscopy (TEM) (Figure 1E). These indentations at the equators indicate that daughter cells of SagA+ enterococci commence cell division before separation from one another. Interestingly, HADA staining (Figure S1A) and TEM (Figure S1B) of various enterococci species encoding SagA orthologs revealed that SagA may broadly contribute to this tri-septal structure. Other *Efs* strains (775 and V583) do not encode SagA-like NlpC/p60 orthologs, but also display faint and pronounced HADA staining at the equators and division septa, respectively (Figure S1A), suggesting the focused HADA staining may be specific to *Efs* OG1RF. Whether the NlpC/p60 domain of SagA plays a structural or catalytic role in this tri-septal phenotype is unclear, as overexpression of the catalytically inactive SagA C443A mutant appeared to be toxic to *Efm* Com15 cells and yielded no colonies, and chromosomal insertion of SagA C443A in *Efs* OG1RF yielded low or undetectable levels of protein expression.[12] Nevertheless, due to the faster growth rate and abundance of non-crosslinked PG in *Efm* Com15 compared to *Efs* OG1RF,[12] it is possible that SagA simultaneously contributes to cell division and separation.

To study the subcellular localization of SagA, we inserted a tetracysteine (Cys4) tag at its C-terminus and ectopically expressed it in *Efm* cells (Figure 2A). We found no significant growth defects in cells overexpressing SagA compared to control cells containing the empty vector (Figure 2B). We then visualized the protein fusion using the biarsenical dye ReAsH, which covalently binds the Cys4 amino acid motif.[15,16] We found that SagA localizes at the septa and equators in dividing *Efm* cells (Figure 2C), further suggesting a regulatory role of SagA in bacterial cell division. We also found SagA C-terminal truncation ($SagA^{\Delta C}$) and SagA N-terminus ($SagA^{Nter}$) localize at the septa and equators using the Cys4-tagging and ReAsH labeling (Figure S2), suggesting that the coiled-coil N-terminal domain is sufficient for the subcellular localization of SagA. The differential colocalization of these two constructs compared to wild-type may be attributed to lower expression in *Efm* (Figure S2D) and may also indicate that correct folding of the full-length protein is important for targeting septal PG.

Protein fold analysis using Phyre2[20] shows that the SagA N-terminus bears 99% secondary structure homology to the inactive, auto-inhibitory module[21] of the essential PG hydrolase PcsB[29] from *Streptococcus pneumoniae*.[21] Structural studies suggest PcsB adopts an interlocking, autoinhibitory dimeric structure where the N-terminal coiled-coil domain of one monomer interacts with the catalytic C-terminus of the other in an inactive conformation.[21] This homology between the N-termini of SagA and PcsB suggests that the SagA N-terminus may have a regulatory function aside from contributing to the subcellular localization of SagA. However, intact protein analysis by MALDI-TOF mass spectrometry revealed that full-length SagA exists in a monomeric state (Figure S3). Additionally, the unusual linker length of SagA (120 amino acids) raises the possibility for the N and C-termini to interact. We were unable to ectopically express an N-terminal truncation of SagA ($SagA^{\Delta Nter}$) in *Efm* Com15 for imaging studies. Therefore, to discern the role of the SagA N-terminus in SagA D,L-endopeptidase activity, we compared the *in vitro* enzymatic activity of recombinant full-length SagA and SagA-NlpC/p60 (Figure 3A) on soluble muramidase-digested *Efs* PG. Full-length SagA and SagA-NlpC/p60 demonstrated comparable D,L-endopeptidase activity towards model PG fragments similar to nascent and template PG in *Efm*[25–27] (Figures 3B–D and S4, Tables S4 and S5). Full-length SagA D,L-endopeptidase activity more readily produced smaller cross-linked fragments ($Product_e$ in Figure 3D and $Product_f$ in Figure S4C), but there was no significant difference in overall GlcNAc-MurNAc-dipeptide production compared to the SagA-NlpC/p60 domain alone (Figure S4E), suggesting that the N-terminus does not play an autoinhibitory role, but perhaps a scaffolding and targeting function in enterococci. Our results also suggest additional enzymes such as muramidases or other glycosidases in *Efm* are needed to generate smaller PG fragments that can then be cleaved by SagA.

To further understand the mechanisms involved in SagA activity, we performed alanine scanning mutagenesis of SagA-NlpC/p60 using our optimized expression and purification protocol from *E. coli*.[17] Our previous studies show that W433 and W462 are required for SagA-NlpC/p60 activity and may contribute to substrate binding based on the SagA-NlpC/p60 structure and modeling studies,[12] but other amino acid residues involved in activity and potential substrate binding have not been evaluated. We therefore performed docking studies of the monomeric pentapeptide PG fragment, GlcNAc-MurNAc-L-Ala-D-isoGln-L-Lys-D-Ala-D-Ala (GlcNAc-M5P) with the SagA-NlpC/p60 x-ray structure using the program Glide (Schrödinger).[22,23] GlcNAc-M5P is a common PG fragment in *Efm* Com15 and the SagA- *Efs* OG1RF with the only difference being the bridge link at L-Lys: D-Asn/D-Asp in the former[27] and L-Ala-L-Ala in the latter.[30] Docking of larger cross-linked PG fragments and products was unsuccessful. The docking of GlcNAc-M5P to SagA-NlpC/p60 was constrained so that the L-Ala-γ-D-isoGln dipeptide in the pentapeptide stem was positioned in proximity to the catalytic Cys443 residue like the L-Ala-γ-D-isoGlu dipeptide in the *Bacillus cereus* YkfC NlpC/p60 structure.[31] The ligand-docked model revealed potential key residues for D,L-endopeptidase activity inside and surrounding the putative substrate binding groove (Figures 4A and S5A). Subsequent alanine scanning of these residues using an in-gel profiling assay to observe the production of GlcNAc-MurNAc-dipeptide[12] demonstrated the impact of these mutations on SagA-NlpC/p60 D,L-endopeptidase activity *in vitro* (Figures 4B,C and S5E).

We then evaluated the activity of individual alanine mutants of the residues in the putative catalytic triad of SagA-NlpC/p60, which showed that the C443A and H494A mutants were inactive. Surprisingly, not only did the H506A mutant retain its activity but it was also slightly more active than wild-type SagA-NlpC/p60 (Figure 4C). The disaccharide moiety of the GlcNAc-M5P docked to a region of the substrate binding groove that contained electropositive residues including Lys436 and Arg448. In the docked structure, these residues formed hydrogen bonds and polar interactions with the carbohydrates, respectively, suggesting a stabilizing role (Figure S5B). Accordingly, mutation of either of these residues to Ala diminished SagA hydrolytic activity. We next examined the residues that lined the solvent exposed binding cleft of the pentapeptide stem. With the docked model oriented as shown in Figures S5C,D, we observed two prominent ridges of the binding cleft. The first half of the top ridge consists of Ser444, Asp442 and Tyr431, which are highly conserved in NlpC/p60 hydrolases and clustered around the catalytic Cys443 in the SagA-NlpC/p60 structure (Figure S5C).[11,32] The S444A mutant showed diminished activity, whereas the D442A and Y431A mutants were inactive (Figure 4C), likely due to the disruption of the interaction of each residue with γ-D-isoGln shown in the docked model (Figure S5C). While Ser444 did not directly bind with the PG stem, Asp442 hydrogen bonded with the amide NH group of γ-D-isoGln.[31,33,34] Moreover, Tyr431 is oriented towards the carbonyl of the γ-D-isoGln-L-Lys amide bond, supporting its proposed function in creating an "oxyanion hole" to stabilize the tetrahedral intermediate formed during catalysis.[32,35–37] The second half of the top ridge consists of Gln509 and Glu512 protruding over the groove, and Lys515 at the seam of the groove (Figure S5C). The observed lower activity of the Q509A mutant may be due to the lack of the hydrogen bond shown between Gln509 and the carboxyl carbonyl of the terminal D-Ala which may help anchor peptide stems in the groove. Surprisingly, the E512A mutant demonstrated enhanced D,L-endopeptidase activity whereas the activity of the K515A mutant was on par with that of the Q509A mutant (Figure 4C). This improved activity for the E512A mutant was interesting, as no direct bond was observed between Glu512 and the terminal D-Ala-D-Ala in the docked model. Likewise, Lys515 did not directly interact with the bound ligand, but it does contribute to an exposed pocket at the seam of the groove, which may be important for proper binding of PG substrates and may explain the weaker activity of the K515A mutant.

In the bottom ridge (Figure S5D), Thr463 is the only polar residue near Cys443, and the abrogated activity of the T463A mutant (Figure 4C) may be due to the disruption of the hydrogen bond formed between the backbone carbonyl of Thr463 and the amino group of γ-D-isoGln. The first aromatic residue in the bottom ridge, Tyr493, is positioned near the branching point of L-Lys and D-Ala-D-Ala in the middle of the groove and the Y493A mutant showed lower activity. *In silico* alanine scanning of Tyr493 using Schrödinger generated the SagA-NlpC/p60 Y493A mutant structure (Figure S6B). The binding groove is more solvent-exposed (Figure S6A,B), which suggests that this aromatic residue may hold the terminal amino acids within the groove via van der Waals interactions. Mutants of residues towards the end of the bottom ridge, F522A and W521A, had similar activity to wild-type, suggesting that these residues are not crucial for activity even though they are positioned near the terminal D-Ala (Figure S5D). In contrast, the V516A mutant exhibited

weaker activity, perhaps because it contributes to the exposed pocket at the seam of the groove like Lys515.

To explain the enhanced activity observed with the H506A and E512A mutants, further *in silico* alanine scanning was performed with particular attention paid to the periphery of the SagA-NlpC/p60. Interestingly, His506 juts into this pocket and Glu512 is directly above it. *In silico* alanine scanning of these residues generated SagA-NlpC/p60 structures with alterations of the pocket: the H506A mutant structure contributed a pronounced cavity to the pocket, thus deepening it (Figure S6C), and the E512A mutant structure flattened the space above the pocket (Figure S6D). Therefore, it is conceivable that these structural alterations allow for better binding and hydrolysis of PG as observed in our *in vitro* activity assays (Figure 4C). Collectively, these results indicate that PG substrates are oriented towards the top ridge of the putative SagA-NlpC/p60 substrate binding groove for proper D,L-endopeptidase activity and production of GlcNAc-MurNAc-dipeptide.

Genomic analysis and primary sequence alignment revealed that the Cys-His-His triad is conserved across multiple SagA orthologs from other enterococci (Figure 5A). To address if SagA-like proteins in general used catalytic dyads or if our finding was unique to *Efm* Com15 SagA, we prepared recombinant Cys-His-Ala mutants of full-length SagA orthologs from *Efm* Com15, *Eds* 2RC2, and *Emi* 2312 (Figure 5B) and evaluated their biochemical activity *in vitro*. Compared to the buffer control and the inactive *Efm* Com15 SagA C443A mutant, all Cys-His-Ala mutants demonstrated D,L-endopeptidase activity (Figures 5C and S7, Tables S4 and S5), suggesting that the conserved second histidine is not required for *in vitro* activity. Inspection of the docked SagA-NlpC/p60 structure did not reveal any obvious residues that may pair with Cys443-His494 to comprise a catalytic triad, thus indicating that SagA-NlpC/p60 may function via a catalytic Cys-His dyad. Although most structurally similar NlpC/p60 hydrolases contain residues for a Cys-His-His catalytic triad in a similar orientation to SagA-NlpC/p60,[12] the functional role of these residues has not been completely established. Therefore, these results suggest that the putative catalytic Cys-His-His triad should be reevaluated for other NlpC/p60 hydrolases. A notable exception is RipA-NlpC/p60, which has a required catalytic Cys-His-Glu triad.[34] The glutamic acid residue is proposed to form a salt bridge with a neighboring arginine residue to lock in the orientation of the catalytic cysteine, which Squeglia et al note an equivalent histidine residue is unable to form.[34] The lack of this interaction in NlpC/p60 domains with a conserved Cys-His-His triad, coupled with the limited flexibility of the catalytic site in these domains,[34] raises the possibility that the second histidine may not have a role in catalysis.

To better understand structural features that govern NlpC/p60 hydrolase function, we compared the topology of the putative SagA-NlpC/p60 substrate binding groove with that of other biochemically and structurally characterized NlpC/p60-type hydrolases. These representative NlpC/p60 hydrolases have varied domain architectures (Figure S8A) and their NlpCp60 domains display a broad range of enzymatic and hydrolytic specificities *in vitro*. Sequence alignment of the NlpCp60 domains show conservation of the SagA-NlpC/p60 core residues (i.e. Y431, D442, C443, S444, H494 and H506), but there is poor similarity of several of the residues that we have demonstrated to modulate the *in vitro* endopeptidase activity of SagA-NlpC/p60 (Figure S8B). However, structural alignment of SagA-NlpC/p60

with these NlpC/p60 domains highlights key differences in their putative binding grooves that may dictate their respective functions (Figures S8C and S9). For instance, unlike SagA-NlpC/p60, the RipA NlpC/p60 domain has a prominent loop occluding its entire binding groove (Figure S9A). This loop is a putative inhibitory prodomain that is proposed to be proteolytically cleaved *in vivo* for activation of RipA at the *M. tuberculosis* septum.[38–42] The *Staphylococcus aureus* CwlT NlpC/p60 domain, on the other hand, shows a loop protruding from its bottom ridge partially blocking the groove near the site of Tyr493 in SagA-NlpC/p60, but it also has a flatter and more open groove periphery (Figure S9B).[35] The *E. coli* Spr NlpC/p60 domain contains a similar loop, but it actually points into the groove, as do several bulky residues at the periphery (Figure S9C).[37] The binding groove of the ligand bound NlpC/p60 domain of *Bacillus cereus* YkfC is slightly more open, except for two features at the beginning and end of the groove (Figure S9D).[31] First, the SH3b1 domain of YkfC blocks the entrance of its NlpC/p60 binding groove, which is proposed to contribute to the substrate specificity of YkfC towards stem peptides with an N-terminal L-Ala (i.e. no disaccharide moiety).[36] Second, Arg309 and Tyr321 of YkfC are positioned near Glu512 and Phe522 in the SagA-NlpC/p60 structure and they occlude the pocket in the YkfC binding groove periphery. Interestingly, the NlpC/p60 domain whose binding groove topology is most similar to SagA-NlpC/p60 is of *M. tuberculosis* RipD (Figure S9E), which is a non-catalytic NlpC/p60 domain that retains its ability to bind PG *in vitro*.[43] Overall, the diversity in the binding groove topologies of these NlpC/p60 hydrolases illustrates the challenge of elucidating the exact structural motifs and substrate-protein interactions that govern their enzymatic and hydrolytic specificities. Nevertheless, our structure-function studies of SagA-NlpC/p60 have identified residues and hotspots in the binding groove that may be involved in NlpC/p60 hydrolase activity, but may not have been identified via sequence homology alone, such as the site of the Tyr493 lid and the less studied binding groove periphery.

In summary, our data indicate that SagA is colocalized with zones of active PG remodeling in enterococci, and that the NlpC/p60 hydrolase activity of SagA may be governed by potential key interactions between septal PG and the putative SagA-NlpC/p60 substrate binding groove. We previously characterized the hydrolytic specificity of SagA as a D,L-endopeptidase with a preference towards cross-linked L-Lys-type PG with penta- and tetrapeptide stems,[12] which comprises nascent and template PG chains during PG biosynthesis in *Efm*.[25–27] Given that *sagA* is essential for *Efm* growth,[13] our discovery of the NlpC/p60 hydrolase activity of SagA[12] and the subcellular localization of SagA at the septa of dividing enterococci cells implicate SagA in PG turnover during cell growth and division. To identify potential key contacts between PG substrates and SagA, we docked a representative GlcNAc-MurNAc-pentapeptide into the putative SagA-NlpC/p60 binding groove and analyzed the potential substrate interacting residues of SagA-NlpC/p60 via alanine scanning *in vitro* and *in silico*. Our structural and biochemical studies suggest that PG substrates are oriented towards the top ridge of the putative SagA-NlpC/p60 substrate binding groove, and that substrate interactions at the periphery of the groove may be important for PG turnover. Moreover, our biochemical analysis suggests that SagA may function via a catalytic Cys-His dyad, which was consistent in full-length SagA orthologs from other enterococci species. While structural alignment of SagA-NlpC/p60 with other

structurally and biochemically characterized NlpC/p60 orthologs exhibits the diversity in their putative substrate binding groove topologies, our studies suggest that substrate interactions at the center and periphery of the grooves may govern PG recognition, binding and hydrolysis. Ultimately, this work highlights how the activity of SagA may be involved in the viability of *Efm* and provides a greater understanding of how SagA generates the defined muropeptides that we have shown to have therapeutic potential.[9,10,12]

Supplementary Material

Refer to Web version on PubMed Central for supplementary material.

ACKNOWLEDGEMENTS

We thank Paul Dominic B. Olinares for intact protein analysis by Matrix-assisted Laser Desorption Time-of-Flight Mass Spectrometry (Brian T. Chait lab, The Rockefeller University). We also thank Deena Oren for assistance with *in silico* residue scanning of SagA-NlpC/p60 (The Rockefeller University Structural Biology Resource Center). J.E. acknowledges support from The Rockefeller University Graduate Program and the National Institutes of Health (T32 A1070084). Y.E. was supported by The Rockefeller University Summer Science Research Program (SSRP). B.K. was supported by Helmsley postdoctoral fellowship. H.C.H. acknowledges support from the National Institutes of Health (NIGMS R01 GM103593 and NCI R01 CA245292) and Kenneth Rainin Foundation Synergy Award.

REFERENCES

(1). Vollmer W, Blanot D, and Pedro MA (2008) Peptidoglycan structure and architecture. FEMS Microbiology Reviews 32, 149–167. [PubMed: 18194336]

(2). Sorbara MT, and Philpott DJ (2011) Peptidoglycan: a critical activator of the mammalian immune system during infection and homeostasis. Immunological Reviews 243, 40–60. [PubMed: 21884166]

(3). Royet J, and Dziarski R (2007) Peptidoglycan recognition proteins: pleiotropic sensors and effectors of antimicrobial defences. Nature Reviews Microbiology 5, nrmicro1620.

(4). Boudreau MA, Fisher JF, and Mobashery S (2012) Messenger Functions of the Bacterial Cell Wall-derived Muropeptides. Biochemistry 51, 2974–2990. [PubMed: 22409164]

(5). Wolf AJ, and Underhill DM (2018) Peptidoglycan recognition by the innate immune system. Nature reviews. Immunology.

(6). Griffin ME, Hespen CW, Wang Y, and Hang HC (2019) Translation of peptidoglycan metabolites into immunotherapeutics. Clin Transl Immunol 8, e1095.

(7). Wyckoff TJ, Taylor JA, and Salama NR (2012) Beyond growth: novel functions for bacterial cell wall hydrolases. Trends in Microbiology 20, 540–547. [PubMed: 22944244]

(8). Vollmer W, Joris B, Charlier P, and Foster S (2008) Bacterial peptidoglycan (murein) hydrolases. FEMS Microbiology Reviews 32, 259–286. [PubMed: 18266855]

(9). Rangan KJ, Pedicord VA, Wang Y-C, Kim B, Lu Y, Shaham S, Mucida D, and Hang HC (2016) A secreted bacterial peptidoglycan hydrolase enhances tolerance to enteric pathogens. Science 353, 1434–1437. [PubMed: 27708039]

(10). Pedicord VA, Lockhart AA, Rangan KJ, Craig JW, Loschko J, Rogoz A, Hang HC, and Mucida D (2016) Exploiting a host-commensal interaction to promote intestinal barrier function and enteric pathogen tolerance. Science Immunology 1.

(11). Anantharaman V, and Aravind L (2002) Evolutionary history, structural features and biochemical diversity of the NlpC/P60 superfamily of enzymes. Genome Biology 4, 1–12.

(12). Kim B, Wang Y-C, Hespen CW, Espinosa J, Salje J, Rangan KJ, Oren DA, Kang J, Pedicord VA, and Hang HC (2019) Enterococcus faecium secreted antigen A generates muropeptides to enhance host immunity and limit bacterial pathogenesis. eLife 8, e45343. [PubMed: 30969170]

(13). Teng F, Kawalec M, Weinstock GM, Hryniewicz W, and Murray BE (2003) An Enterococcus faecium Secreted Antigen, SagA, Exhibits Broad-Spectrum Binding to Extracellular Matrix Proteins and Appears Essential for E. faecium Growth. Infect Immun 71, 5033–5041. [PubMed: 12933846]

(14). Hullahalli K, Rodrigues M, and Palmer KL (2017) Exploiting CRISPR-Cas to manipulate Enterococcus faecalis populations. Elife 6, e26664. [PubMed: 28644125]

(15). Adams SR, Campbell RE, Gross LA, Martin BR, Walkup GK, Yao Y, Llopis J, and Tsien RY (2002) New Biarsenical Ligands and Tetracysteine Motifs for Protein Labeling in Vitro and in Vivo: Synthesis and Biological Applications. J Am Chem Soc 124, 6063–6076. [PubMed: 12022841]

(16). Copeland MF, Flickinger ST, Tuson HH, and Weibel DB (2009) Studying the Dynamics of Flagella in Multicellular Communities of Escherichia coli by Using Biarsenical Dyes. Appl Environ Microb 76, 1241–1250.

(17). Kim B, Espinosa J, and Hang HC (2020) Biochemical analysis of NlpC/p60 peptidoglycan hydrolase activity. Methods Enzymol.

(18). Fenyo D, Wang Q, DeGrasse JA, Padovan JC, Cadene M, and Chait BT (2007) MALDI sample preparation: the ultra thin layer method. J Vis Exp Jove 192. [PubMed: 18978997]

(19). Cadene M, and Chait BT (2000) A Robust, Detergent-Friendly Method for Mass Spectrometric Analysis of Integral Membrane Proteins. Anal Chem 72, 5655–5658. [PubMed: 11101244]

(20). Kelley LA, Mezulis S, Yates CM, Wass MN, and Sternberg MJE (2015) The Phyre2 web portal for protein modeling, prediction and analysis. Nat Protoc 10, 845–858. [PubMed: 25950237]

(21). Bartual SG, Straume D, Stamsås G, Muñoz IG, Alfonso C, Martínez-Ripoll M, Håvarstein L, and Hermoso JA (2014) Structural basis of PcsB-mediated cell separation in Streptococcus pneumoniae. Nature Communications 5, 3842.

(22). Friesner RA, Banks JL, Murphy RB, Halgren TA, Klicic JJ, Mainz DT, Repasky MP, Knoll EH, Shelley M, Perry JK, Shaw DE, Francis P, and Shenkin PS (2004) Glide: A New Approach for Rapid, Accurate Docking and Scoring. 1. Method and Assessment of Docking Accuracy. J Med Chem 47, 1739–1749. [PubMed: 15027865]

(23). Halgren TA, Murphy RB, Friesner RA, Beard HS, Frye LL, Pollard WT, and Banks JL (2004) Glide: A New Approach for Rapid, Accurate Docking and Scoring. 2. Enrichment Factors in Database Screening. J Med Chem 47, 1750–1759. [PubMed: 15027866]

(24). Lyne PD, Lamb ML, and Saeh JC (2006) Accurate Prediction of the Relative Potencies of Members of a Series of Kinase Inhibitors Using Molecular Docking and MM-GBSA Scoring. J Med Chem 49, 4805–4808. [PubMed: 16884290]

(25). Patti GJ, Kim SJ, and Schaefer J (2008) Characterization of the Peptidoglycan of Vancomycin-Susceptible Enterococcus faecium †. Biochemistry-us 47, 8378–8385.

(26). Patti GJ, Chen J, and Gross ML (2009) Method Revealing Bacterial Cell-Wall Architecture by Time-Dependent Isotope Labeling and Quantitative Liquid Chromatography/Mass Spectrometry. Analytical Chemistry 81, 2437–2445. [PubMed: 19281243]

(27). Patti GJ, Chen J, Schaefer J, and Gross ML (2008) Characterization of Structural Variations in the Peptidoglycan of Vancomycin-Susceptible Enterococcus faecium: Understanding Glycopeptide–Antibiotic Binding Sites Using Mass Spectrometry. Journal of the American Society for Mass Spectrometry 19, 1467–1475. [PubMed: 18692403]

(28). Parker MFL, Flavell RR, Luu J, Rosenberg OS, Ohliger MA, and Wilson DM (2020) Small molecule sensors targeting the bacterial cell wall. Acs Infect Dis.

(29). Ng W-L, Kazmierczak KM, and Winkler ME (2004) Defective cell wall synthesis in Streptococcus pneumoniae R6 depleted for the essential PcsB putative murein hydrolase or the VicR (YycF) response regulator: Defective cell wall synthesis in pcsB mutants. Mol Microbiol 53, 1161–1175. [PubMed: 15306019]

(30). Emirian A, Fromentin S, Eckert C, Chau F, Dubost L, Delepierre M, Gutmann L, Arthur M, and Mesnage S (2009) Impact of peptidoglycan O-acetylation on autolytic activities of the Enterococcus faecalis N-acetylglucosaminidase AtlA and N-acetylmuramidase AtlB. FEBS Letters 583, 3033–3038. [PubMed: 19686739]

(31). Xu Q, Abdubek P, Astakhova T, Axelrod HL, Bakolitsa C, Cai X, Carlton D, Chen C, Chiu H-J, Chiu M, Clayton T, Das D, Deller MC, Duan L, Ellrott K, Farr CL, Feuerhelm J, Grant JC, Grzechnik A, Han G, Jaroszewski L, Jin KK, Klock HE, Knuth MW, Kozbial P, Krishna SS, Kumar A, Lam WW, Marciano D, Miller MD, Morse AT, Nigoghossian E, Nopakun A, Okach L, Puckett C, Reyes R, Tien HJ, Trame CB, Bedem H. van den, Weekes D, Wooten T, Yeh A, Hodgson KO, Wooley J, Elsliger M-A, Deacon AM, Godzik A, Lesley SA, and Wilson IA (2010) Structure of the γ-d-glutamyl-l-diamino acid endopeptidase YkfC from Bacillus cereus in complex with l-Ala-γ-d-Glu: insights into substrate recognition by NlpC/P60 cysteine peptidases. Acta Crystallographica Section F: Structural Biology and Crystallization Communications 66, 1354–1364. [PubMed: 20944232]

(32). Xu Q, Sudek S, McMullan D, Miller MD, Geierstanger B, Jones DH, Krishna SS, Spraggon G, Bursalay B, Abdubek P, Acosta C, Ambing E, Astakhova T, Axelrod HL, Carlton D, Caruthers J, Chiu H-J, Clayton T, Deller MC, Duan L, Elias Y, Elsliger M-A, Feuerhelm J, Grzechnik SK, Hale J, Han G, Haugen J, Jaroszewski L, Jin KK, Klock HE, Knuth MW, Kozbial P, Kumar A, Marciano D, Morse AT, Nigoghossian E, Okach L, Oommachen S, Paulsen J, Reyes R, Rife CL, Trout CV, Bedem H. van den, Weekes D, White A, Wolf G, Zubieta C, Hodgson KO, Wooley J, Deacon AM, Godzik A, Lesley SA, and Wilson IA (2009) Structural Basis of Murein Peptide Specificity of a γ-D-Glutamyl-L-Diamino Acid Endopeptidase. Structure 17, 303–313. [PubMed: 19217401]

(33). Fukushima T, Kitajima T, Yamaguchi H, Ouyang Q, Furuhata K, Yamamoto H, Shida T, and Sekiguchi J (2008) Identification and Characterization of Novel Cell Wall Hydrolase CwlT A TWO-DOMAIN AUTOLYSIN EXHIBITING N-ACETYLMURAMIDASE AND dl-ENDOPEPTIDASE ACTIVITIES. Journal of Biological Chemistry 283, 11117–11125.

(34). Squeglia F, Ruggiero A, Romano M, Vitagliano L, and Berisio R (2014) Mutational and structural study of RipA, a key enzyme in Mycobacterium tuberculosis cell division: evidence for the l-to-d inversion of configuration of the catalytic cysteine. Acta Crystallographica Section D: Biological Crystallography 70, 2295–300. [PubMed: 25195744]

(35). Xu Q, Chiu H-J, Farr CL, Jaroszewski L, Knuth MW, Miller MD, Lesley SA, Godzik A, Elsliger M-A, Deacon AM, and Wilson IA (2014) Structures of a Bifunctional Cell Wall Hydrolase CwlT Containing a Novel Bacterial Lysozyme and an NlpC/P60 dl-Endopeptidase. Journal of Molecular Biology 426, 169–184. [PubMed: 24051416]

(36). Xu Q, Mengin-Lecreulx D, Liu XW, Patin D, Farr CL, Grant JC, Chiu H-J, Jaroszewski L, Knuth MW, Godzik A, Lesley SA, Elsliger M-A, Deacon AM, and Wilson IA (2015) Insights into Substrate Specificity of NlpC/P60 Cell Wall Hydrolases Containing Bacterial SH3 Domains. mBio 6, e02327–14. [PubMed: 26374125]

(37). Aramini JM, Rossi P, Huang YJ, Zhao L, Jiang M, Maglaqui M, Xiao R, Locke J, Nair R, Rost B, Acton TB, Inouye M, and Montelione GT (2008) Solution NMR structure of the NlpC/P60 domain of lipoprotein Spr from Escherichia coli: structural evidence for a novel cysteine peptidase catalytic triad. Biochemistry 47, 9715–7. [PubMed: 18715016]

(38). Chao MC, Kieser KJ, Minami S, Mavrici D, Aldridge BB, Fortune SM, Alber T, and Rubin EJ (2013) Protein complexes and proteolytic activation of the cell wall hydrolase RipA regulate septal resolution in mycobacteria. Plos Pathog 9, e1003197. [PubMed: 23468634]

(39). Böth D, Schneider G, and Schnell R (2011) Peptidoglycan Remodeling in Mycobacterium tuberculosis: Comparison of Structures and Catalytic Activities of RipA and RipB. Journal of Molecular Biology 413, 247–260. [PubMed: 21864539]

(40). Ruggiero A, Marasco D, Squeglia F, Soldini S, Pedone E, Pedone C, and Berisio R (2010) Structure and Functional Regulation of RipA, a Mycobacterial Enzyme Essential for Daughter Cell Separation. Structure 18, 1184–1190. [PubMed: 20826344]

(41). Squeglia F, Moreira M, Ruggiero A, and Berisio R (2019) The Cell Wall Hydrolytic NlpC/P60 Endopeptidases in Mycobacterial Cytokinesis: A Structural Perspective. Cells 8, 609.

(42). Martinelli DJ, and Pavelka MS (2016) The RipA and RipB Peptidoglycan Endopeptidases Are Individually Nonessential to Mycobacterium smegmatis. Journal of Bacteriology 198, 1464–1475. [PubMed: 26977111]

(43). Böth D, Steiner E, Izumi A, Schneider G, and Schnell R (2014) RipD (Rv1566c) from Mycobacterium tuberculosis: adaptation of an NlpC/p60 domain to a non-catalytic peptidoglycan-binding function. Biochem J 457, 33–41. [PubMed: 24107184]

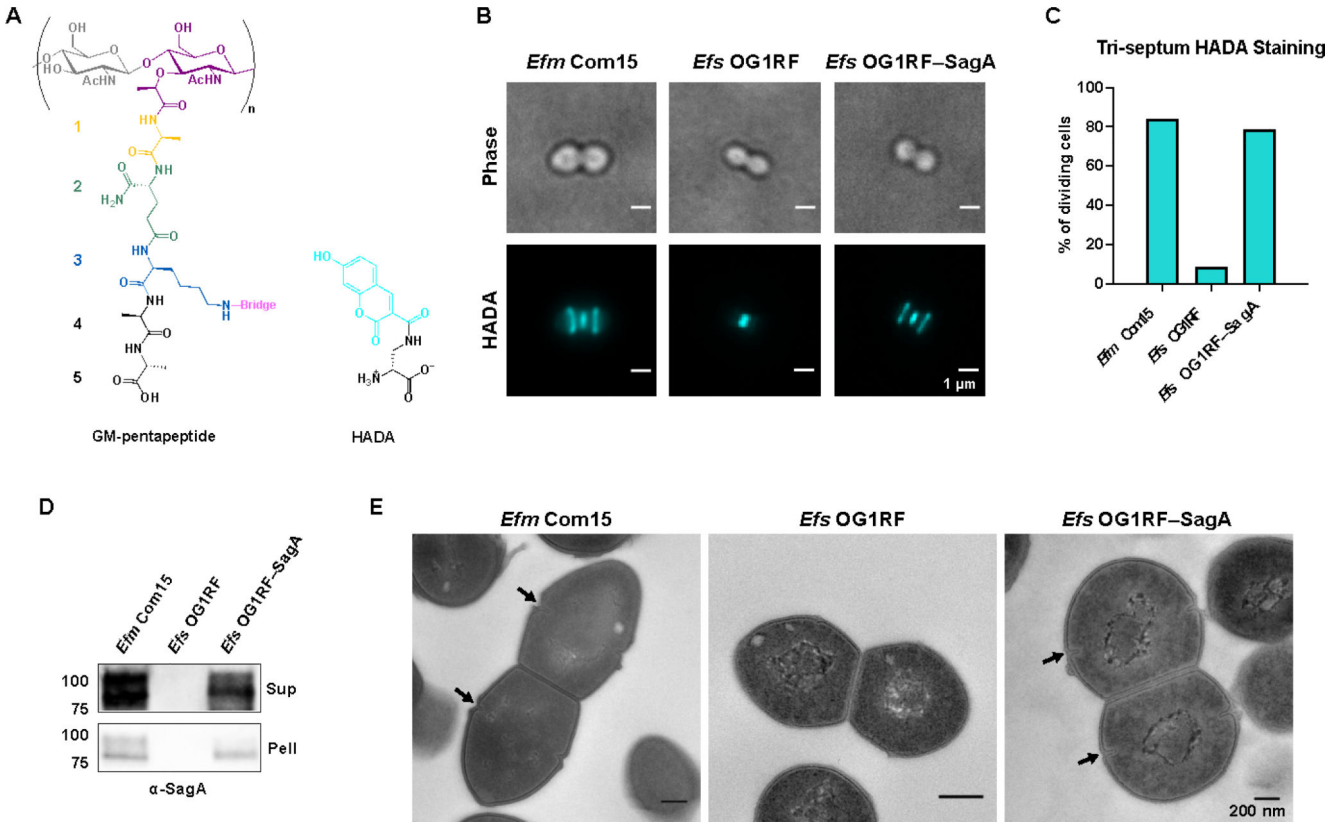

Figure 1. SagA contributes to tri-septum HADA staining in dividing cells.

(A) Chemical structures of GM-pentapeptide (GlcNAc-MurNAc-L-Ala-D-isoGln-L-Lys-D-Ala-D-Ala, left) and HADA (right). For GM-pentapeptide, the position of each amino acid in the peptide stem is numbered on the left. The covalent bridge on the L-Lys is most often D-Asn/Asp in SagA+ enterococci, or L-Ala-L-Ala in *Enterococcus faecalis* strains. (B) HADA staining of enterococci. Scale bar = 1 μm. (C) Percentage of dividing cells with tri-septum HADA staining. 300 cells counted for each strain. (D) Expression of SagA confirmed by α-SagA immunoblotting of culture media supernatant (Sup) and cell pellet lysate (Pell). (E) TEM imaging reveals obvious tri-septum indentations (arrows) in SagA+ enterococci (*Efm* Com15 and *Efs* OG1RF–SagA), but not in SagA- enterococci (*Efs* OG1RF). Scale bar = 200 nm. *Efm* Com15, *Enterococcus faecium* Com15; *Efs* OG1RF, *Enterococcus faecalis* OG1RF; *Efs* OG1RF–SagA, *Enterococcus faecalis* OG1RF–SagA chromosomal insertion.

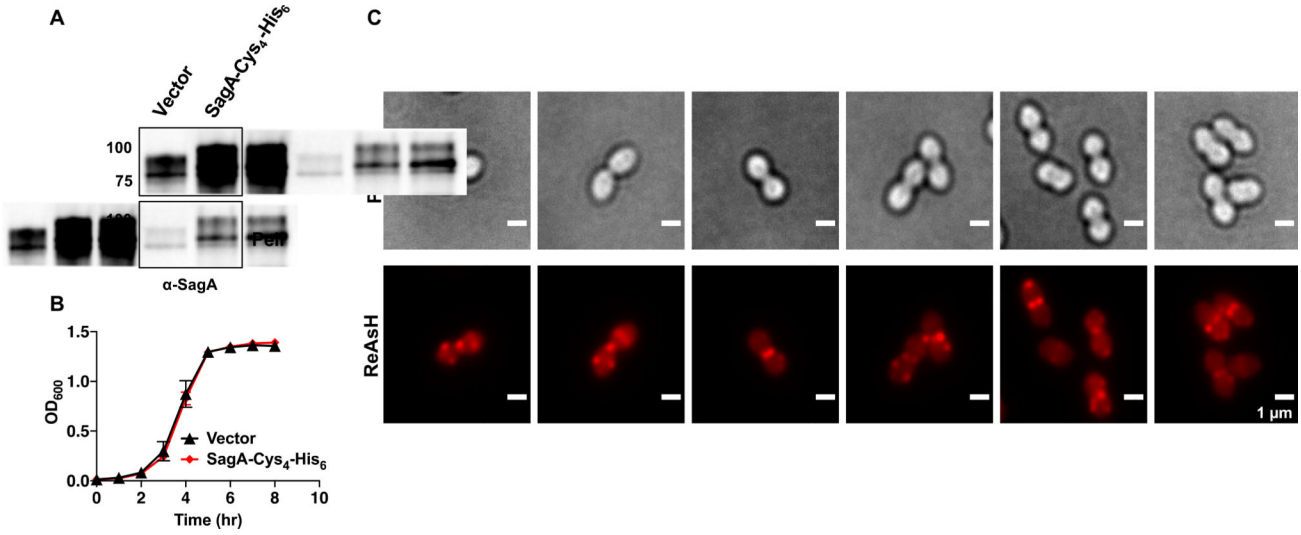

Figure 2. SagA is localized at the cell division site of *E. faecium* Com15.

(A) Expression of SagA confirmed by α-SagA immunoblotting of culture media supernatant (Sup) and cell pellet lysate (Pell). (B) Growth curve of *E. faecium* Com15 strains (n = 6). (C) Fluorescence microscopy of *E. faecium* Com15 overexpressing SagA-Cys_4-His_6. Scale bar = 1 μm. Vector, *E. faecium* Com15 transformed with empty pAM401 overexpression vector; SagA-Cys_4-His_6, *E. faecium* Com15 transformed with pAM401:SagA-Cys_4-His_6 overexpression vector.

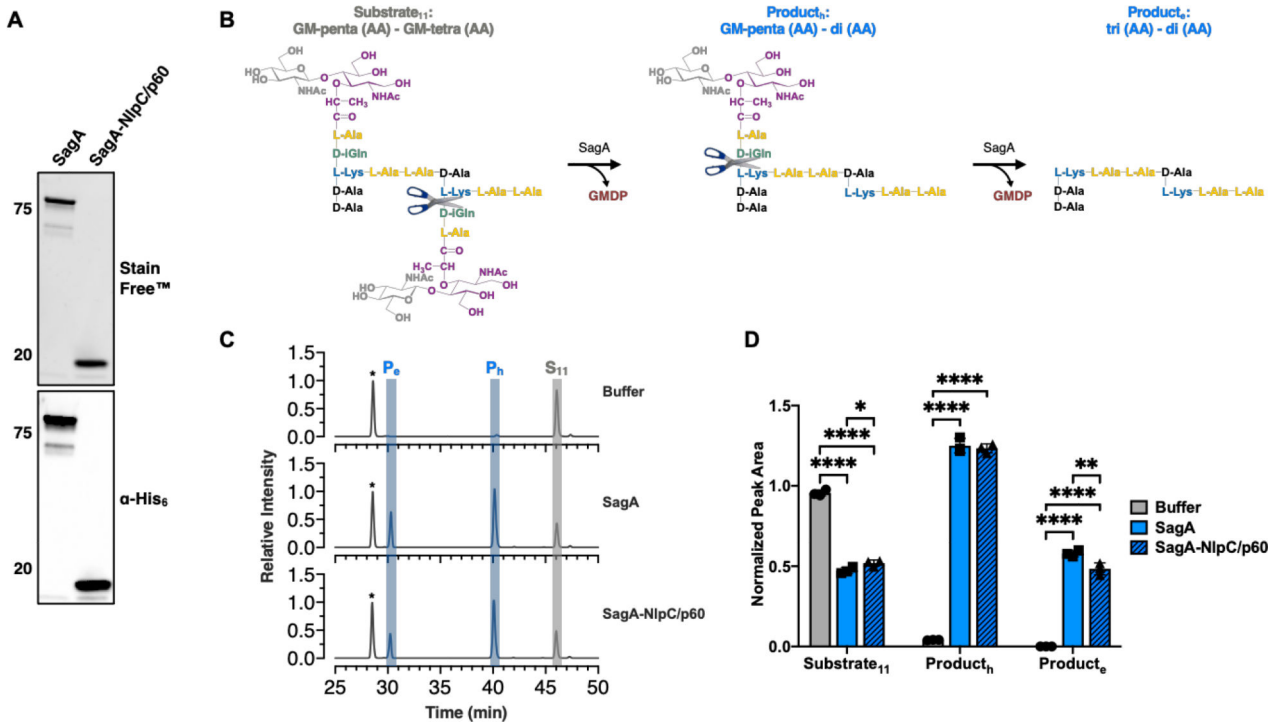

Figure 3. Comparison of *in vitro* activity of SagA truncation constructs.

(A) Stain-Free (Bio-Rad) SDS-PAGE and α-His_6 immunoblotting of SagA constructs purified from the cell-free lysate of BL21(DE3)-RIL *Escherichia coli*. (B) Schematic of *in vitro* SagA D,L-endopeptidase activity. $Substrate_{11}$ represents the most abundant of the soluble, cross-linked muropeptides released following mutanolysin digestion of intact *E. faecalis* OG1RF PG. Iterative cleavage of $Substrate_{11}$ by SagA generates GlcNAc-MurNAc-dipeptide (GMDP) and two fragments, $Product_h$ and $Product_e$. $Substrate_{11}$ and $Product_h$ are illustrated with reduced anomeric carbon of MurNAc. Numbers and letters in subscript denote the LC-MS peak labels described in Tables S4 and S5, respectively. (C) LC-MS analysis of soluble mutanolysin-digested *E. faecalis* OG1RF PG incubated with buffer, SagA, or SagA-NlpC/p60 at 37°C for 16 hr. Data are shown as extracted ion chromatograms. The intensity of extracted ion abundance was normalized to the unchanging GM-tripeptide (AA) peak marked with an asterisk. Colored columns indicate PG substrate and products as described in panel (B). See Figure S4 for the corresponding total ion chromatograms. (D) Quantification of substrate depletion and product formation by SagA truncation constructs *in vitro* (n = 3). For each condition, peak areas were recorded from extracted ion chromatograms of substrate and products and normalized to that of the unchanging GM-tri-(AA). Data were analyzed with one-way ANOVA and Tukey's multiple comparisons post-hoc test. Centerline, average. Error bar, SD ****$P < 0.0001$, ***$P < 0.0002$, **$P < 0.0021$. Comparisons with no asterisk had $P > 0.05$ and were not considered significant.

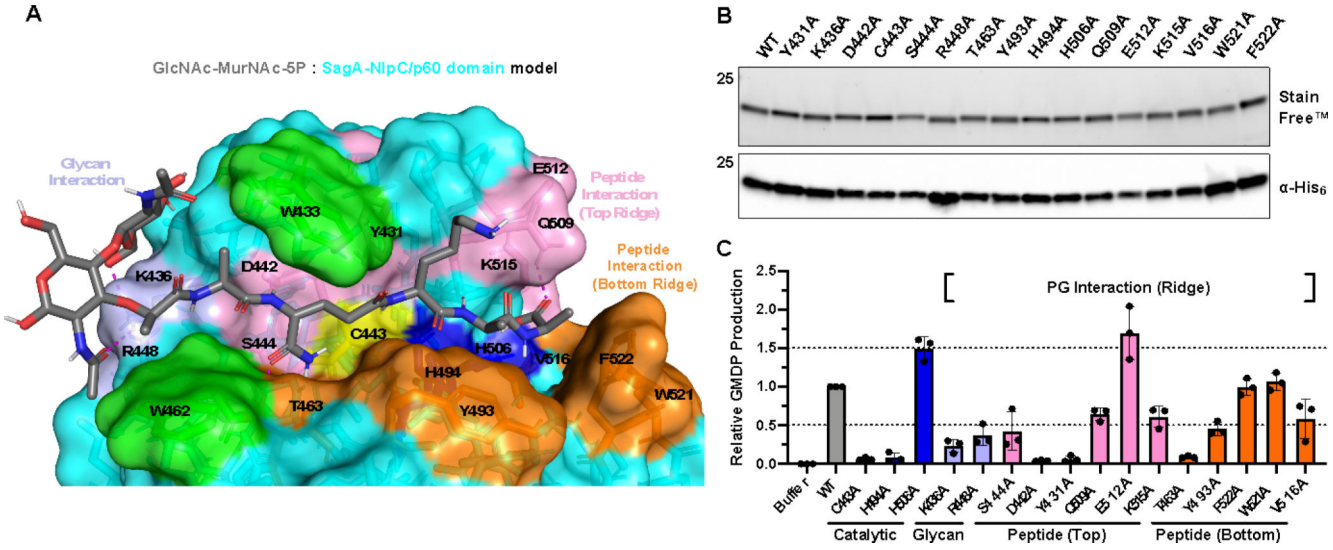

Figure 4. Alanine scanning of the putative SagA-NlpC/p60 substrate binding groove reveals key residues for endopeptidase activity *in vitro*.

(A) Model of GlcNAc-MurNAc-pentapeptide (5P = L-Ala-D-isoGln-L-Lys-D-Ala-D-Ala) docked into the SagA-NlpC/p60 structure with optimized hydrogen bonding network at pH 7.0 using Glide (Schrödinger, LLC, New York, NY). Residues in the putative SagA-NlpC/p60 binding groove with potential interactions with PG are highlighted: positively charged residues at the entrance of the groove (lavender, glycan interaction); mostly polar and charged residues along the top ridge of the binding groove (pink, peptide interaction); mostly aromatic residues along the bottom ridge of the binding groove (orange, peptide interaction). Putative catalytic triad of Cys443 (yellow), His494 (blue), His506 (blue), and the required Trp433 (green), and Trp462 (green) are highlighted. Hydrogen bonding marked by dashed magenta lines. (B) Stain-Free (Bio-Rad) SDS-PAGE and α-His_6 immunoblotting of SagA-NlpC/p60 alanine mutants purified from the cell-free lysate of BL21(DE3)-RIL *Escherichia coli*. (C) Quantification of relative GlcNAc-MurNAc-dipeptide (GMDP) production by SagA-NlpC/p60 alanine mutants. Mutanolysin-digested *E. faecalis* OG1RF PG was incubated with buffer or SagA-NlpC/p60 alanine mutants at 37°C for 16 hr, followed by incubation of the reaction mixture with ANTS fluorophore at 37°C for 16 hr and in-gel profiling of the PG fragments. Intensities of the GMDP product bands were recorded and normalized to the WT band intensity (n = 3). Columns are highlighted according to docked model in panel (A). Top horizontal line, ≥ 50% WT activity. Bottom horizontal line, ≤ 50% WT activity. Column centerline, average. Error bar, SD.

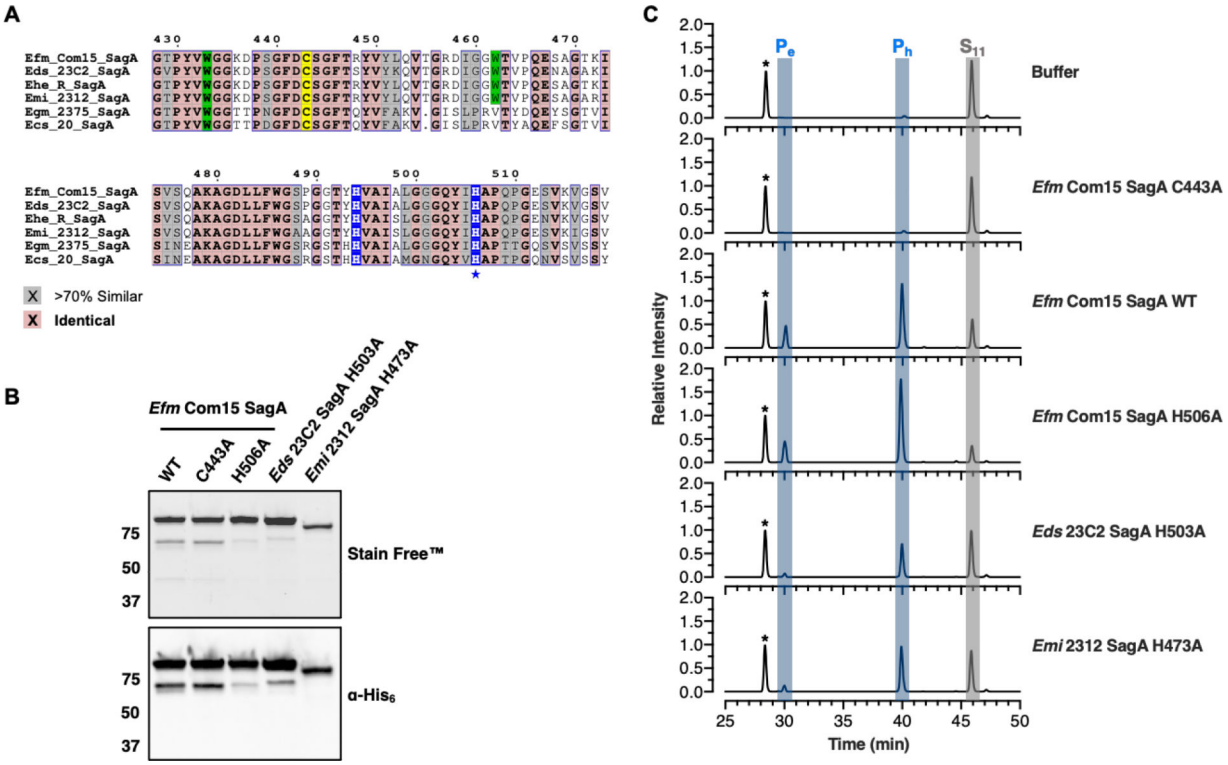

Figure 5. Conserved His506 not required for in vitro activity of SagA orthologs from other enterococci.

(A) Multiple sequence alignment of *Efm* Com15 SagA-NlpC/p60 with the NlpC/p60 domains of SagA orthologs. SagA ortholog sequences were located downstream of *mreD* locus using BioCyc. NlpC/p60 domains were determined using InterPro. Multiple sequence alignment was performed using ClustalOmega and analyzed with ESPript. Conserved H506 marked with blue star (B) Stain-Free (Bio-Rad) SDS-PAGE and α-His_6 immunoblotting of SagA orthologs purified from the cell-free lysate of BL21(DE3)-RIL *Escherichia coli*. (C) LC-MS analysis of soluble mutanolysin-digested *E. faecalis* OG1RF PG incubated with buffer or full-length SagA orthologs at 37°C for 16 hr. Data are shown as extracted ion chromatograms with colored columns representing $Substrate_{11}$, $Product_h$, and $Product_e$, as in Figure 3B,C. See Figure S7 for the corresponding total ion chromatograms. *Efm* Com15, *E. faecium* Com15; *Eds* 23C2, *E. durans* 23C2; *Ehe* R, *E. hirae* R; *Emi* 2312, *E. mundtii* NCDO 2312; *Egm* 2375, *E. gallinarum* NCDO 2375; *Ecs* 20, *E. casseliflavus* 20.